

Communication

Multi-Lane Mirror for Broadband Applications of the Betatron X-ray Source

Marek Raclavský^{1,2}, Krishna P. Khakurel^{1,*}, Uddhab Chaulagain¹, Marcel Lamač^{1,3} and Jaroslav Nejd1¹

¹ Institute of Physics, ELI Beamlines, Academy of Sciences of the Czech Republic, Na Slovance 1999/2, 18221 Prague, Czech Republic; Marek.Raclavsky@eli-beams.eu (M.R.); Uddhab.Chaulagain@eli-beams.eu (U.C.); Marcel.Lamac@eli-beams.eu (M.L.); Jaroslav.Nejdl@eli-beams.eu (J.N.)

² FNSPE, Czech Technical University in Prague, Břehová 78/7, 11519 Prague, Czech Republic

³ Faculty of Mathematics and Physics, Charles University, Ke Karlovu 3, 12116 Prague, Czech Republic

* Correspondence: Krishna.Khakurel@eli-beams.eu

Abstract: A new generation of small-scale ultrafast X-ray sources is rapidly emerging. Laser-driven betatron radiation represents an important class of such ultrafast X-ray sources. With the sources driving towards maturity, many important applications in material and biological sciences are expected to be carried out. While the last decade mainly focused on the optimization of the source properties, the development of such sources into user-oriented beamlines in order to explore the potential applications has recently taken off and is expected to grow rapidly. An important aspect in the realization of such beamlines will be the implementation of proper X-ray optics. Here, we present the design of a multi-lane X-ray mirror as a versatile focusing device covering a wide spectral range of betatron X-rays. The expected photon flux in the focal plane of such optics was also estimated through geometrical simulations.

Keywords: ultrafast X-rays; betatron X-rays; multi-lane KB mirrors



Citation: Raclavský, M.; Khakurel, K.P.; Chaulagain, U.; Lamač, M.; Nejd1, J. Multi-Lane Mirror for Broadband Applications of the Betatron X-ray Source. *Photonics* **2021**, *8*, 579. <https://doi.org/10.3390/photonics8120579>

Received: 17 November 2021

Accepted: 13 December 2021

Published: 15 December 2021

Publisher's Note: MDPI stays neutral with regard to jurisdictional claims in published maps and institutional affiliations.



Copyright: © 2021 by the authors. Licensee MDPI, Basel, Switzerland. This article is an open access article distributed under the terms and conditions of the Creative Commons Attribution (CC BY) license (<https://creativecommons.org/licenses/by/4.0/>).

1. Introduction

X-ray science has made significant advances with the introduction of the femtosecond X-ray sources. Novel applications in material and biological sciences are being explored with such sources [1–3]. Until recently, the use of ultrafast X-rays in materials and biological sciences has been mainly limited to X-ray free-electron lasers (XFELs). Such sources are few in number across the world and hence offer only limited access to users. Recently, significant interest in the development of complementary laser-driven small-scale ultrafast X-ray sources has been magnified. These sources offer unique opportunities to explore ultrafast phenomena in fundamental material and biological sciences. Additionally, the possibility of generating pump beams from the same driving laser makes such sources suitable for following the ultrafast processes in the samples while minimizing the timing jitter, which is challenging in large-scale facilities such as XFELs.

The plasma betatron is a type of small-scale laser-driven ultrafast X-ray source [4–6], based on laser wakefield acceleration (LWFA) [7]. In LWFA, the ponderomotive force drives the plasma wave in which the electrons are trapped and accelerated to relativistic energies when an intense laser ($I > 10^{18} \text{ Wcm}^{-2}$) interacts with underdense plasma (electron density in the range $10^{17}–10^{19} \text{ cm}^{-3}$). Off-axis longitudinal or transverse injection leads to electrons experiencing lateral restoring force due to space-charge separations, which prompts them to execute transverse oscillations as they are accelerated. This oscillatory motion generates bright X-rays (betatron radiation) with characteristics similar to that of synchrotron (wiggler) radiation [4]. The key advantage they offer is that the X-ray pulses are of a few femtoseconds in duration. Furthermore, the source size of the betatron is of the order of microns, which provides a high degree of spatial coherence, and the X-rays are

emitted in a small cone with the divergence of a few tens of mrad. The beam divergence can be further reduced to ~ 5 mrad by using passive plasma lensing [8]. Additionally, the spectrum from the betatron radiation has no characteristic peak and has photon energies ranging from a few eV to tens of keV. The spectrum of betatron X-rays is characterized in terms of critical energy, which is a function of the driving laser pulse energy and the plasma density. Hence, betatron X-rays also offer the unique capability of tuning the X-ray spectrum. Recent experimental scaling showed that using a PW-class laser, which will also be the driving laser at ELI Beamlines, betatron X-ray flux can reach 10^{12} photons/shot [9]. Various numerical and experimental schemes show that the photon flux can be further enhanced by either modifying the gas density profile [10] or using multiple laser beams [11].

A user-oriented multidisciplinary hard X-ray beamline, named the Gammatron beamline, with the plasma betatron as one of the X-ray generation schemes is being developed at the ELI Beamlines facility. Using the high-repetition rate PW laser (up to 30 J, 10 Hz) [12] available at the facility and optimizing the laser and plasma conditions, betatron X-rays with flux as good as 10^{13} photons per shot can be generated. A detailed description of the Gammatron beamline is provided elsewhere [13]. The broadband, collimated, and partially coherent X-rays from betatron radiation make it an ideal source for diverse applications ranging from industrial imaging [14] and phase-contrast imaging [15] to femtosecond time-resolved spectroscopy [16] and diffraction. The X-ray photon flux at a given energy range is one of the parameters that needs to be highly optimized according to the requirements of the chosen application. After the optimization of the source, the optimization of the flux can be achieved only through a properly chosen optical system downstream of the source. Hence, each experiment focusing on a unique application demands a new set of X-ray focusing systems. For instance, the spectroscopic studies of the absorption edges of the light elements would require the lower energy part of the spectrum while the one probing heavier elements would require higher photon energy. Similarly, imaging bulk specimens can be performed only with harder X-ray radiation. Diffraction of both organic and inorganic specimens should be tuned to optimize the scattering cross-section of the element in the specimen. The design, installation, and alignment of X-ray optics for each experiment would not be a time-consuming job for an experimental station focused on optimizing one particular type of experiment. However, for user-orientated betatron X-ray sources such as the ones being developed at ELI Beamlines, this would consume a large fraction of the user experimental time.

In this article, we propose a multi-lane X-ray mirror system to address this problem. The mirror system provides optimal photon guidance for a broad energy spectrum. Each lane of the mirror was optimized for a different spectral range. We designed the optical system in such a way that each mirror-lane had a reflectance $> 60\%$ at a reasonably high grazing incidence angle of 5 mrad covering the spectral range from 1–23 keV. In addition, we predicted the expected number of photons at the sample plane for the entire bandwidth with the help of 3D particle-in-cell (PIC) and geometrical X-ray optics simulations.

2. Simulation

A schematic of the experimental setup for the betatron radiation being developed at the ELI Beamlines is shown in Figure 1. The laser used for generating X-rays has a central wavelength of 808 nm, a pulse duration of 28 fs in full-width at half-maximum (FWHM), and a pulse energy of 10 J. The pulses with a 10 Hz repetition rate are focused onto a spot of a diameter of $16.5 \mu\text{m}$ (FWHM), providing a vacuum intensity of 10^{20} Wcm^{-2} . The laser-target interaction was simulated using PIC code, the results of which were post-processed in order to calculate the generated X-ray radiation.

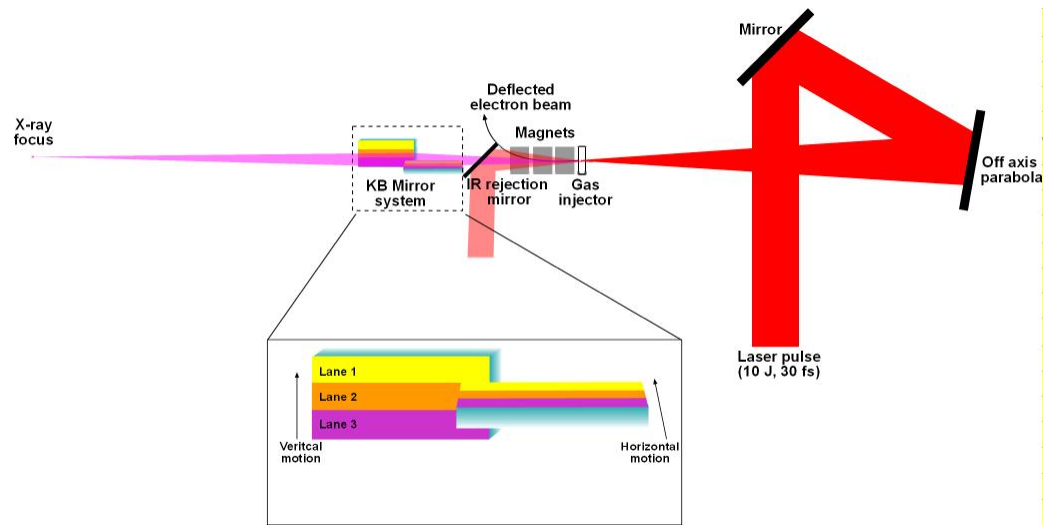


Figure 1. Schematic of the experimental setup. The inset shows the image of the multi-lane KB mirror system.

2.1. Particle-in-Cell and X-ray Emission Simulations

To emulate the experimental performance of the X-ray focusing optics, we simulated the betatron X-ray generation for experimentally accessible parameters with the fully relativistic, massively parallelized three-dimensional (3D) particle-in-cell code EPOCH [17]. For the simulations, the moving window simulation box was set as $80 \mu\text{m} \times 60 \mu\text{m} \times 60 \mu\text{m}$ with a grid size $1200 \times 160 \times 160$ and 2 macro-particles per cell, which corresponds to 12 cells per laser wavelength to achieve a satisfactory resolution of all involved wave-lengths. The laser radiation was linearly polarized along the horizontal direction with parameters described in the earlier part of this report. The laser pulse was focused on the entrance into the 5 mm-long homogeneous pre-ionized helium gas target with smooth edges and a plateau value of electron density of $5 \times 10^{18} \text{cm}^{-3}$. The laser intensity and plasma density were set to result in almost immediate self-injection of electrons into the laser wakefield, leading to the acceleration of the electrons up to 700 MeV. The trajectories, spectrum, and divergence of the accelerated electrons are shown in Figures 2 and 3a,b, respectively. The total charge of the accelerated bunch corresponds to 7 nC or 4.4×10^{10} total accelerated electrons. We further calculated the radiation emitted by the electrons by numerically integrating the angularly resolved spectral distribution of the energy [18]:

$$\frac{d^2W}{d\Omega d\omega} = \frac{e^2}{16\pi^3\epsilon_0 c} \left| \int_{-\infty}^{\infty} \frac{\mathbf{n} \times ((\mathbf{n} - \boldsymbol{\beta}) \times \dot{\boldsymbol{\beta}})}{(1 - \mathbf{n} \cdot \boldsymbol{\beta})^2} e^{i\omega(1 - \mathbf{n} \cdot \mathbf{R}/c)} dt \right|^2. \quad (1)$$

The features of the emitted radiation are presented in Figure 4. The spectrum has a distinct synchrotron shape with a critical energy of 11.5 keV and an FWHM divergence of $30 \text{ mrad} \times 30 \text{ mrad}$. The total energy in the X-ray pulse is 5.6 mJ. The source size is $6 \mu\text{m}$, being the lateral extension of electron oscillations (see Figure 2). The X-ray pulse duration is given by the longitudinal size of the electron bunch, which is roughly $5 \mu\text{m}$. Therefore, the X-ray pulse is as short as 10 fs. The total number of X-ray photons over the full spectrum is 10^{13} photons/shot. Considering a 10 Hz operation, the source results in a betatron flux of 10^{14} photons/s. This gives us a peak brightness of the X-ray betatron source of 3×10^{25} photons/(s mrad² mm² 0.1%BW), making it a competitive alternative to conventional synchrotron sources in terms of flux, but with the added benefit of ultrashort pulses.

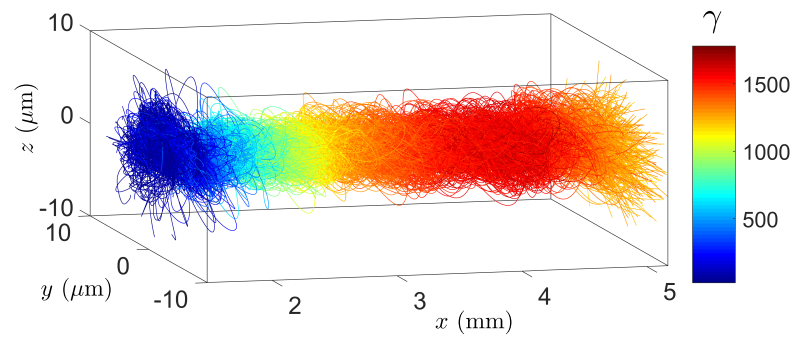


Figure 2. Trajectories of the accelerated electrons.

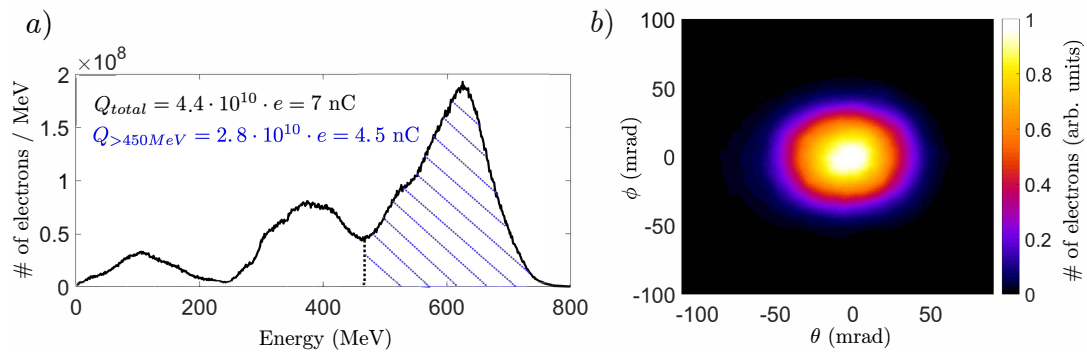


Figure 3. (a) Spectrum and (b) divergence of the accelerated electrons.

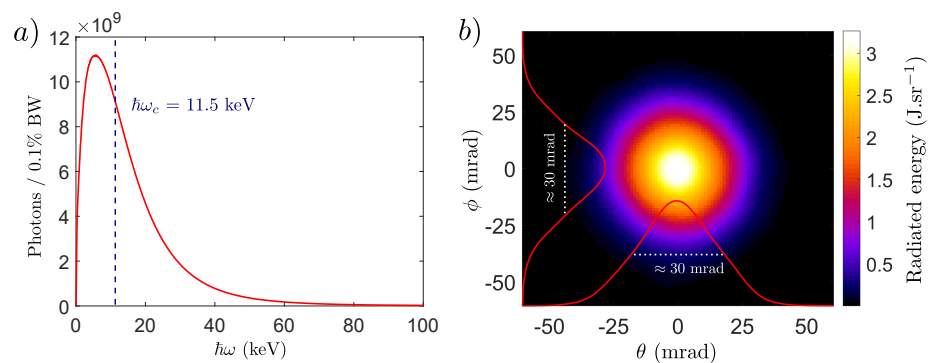


Figure 4. (a) Spectrum and (b) divergence of the emitted X-ray radiation.

2.2. Multi-Lane Mirror System

The mirror system discussed here is shown in Figure 1, and a close-up view is shown in the inset of Figure 1, while a detailed view including the geometrical parameters is depicted in Figure 5. The mirror system comprises two reflecting elliptical surfaces (horizontal and vertical), each consisting of three $20 \text{ cm} \times 1 \text{ cm}$ stripes of Ir/Cr coating, either bilayer or multilayer. The two, horizontal and vertical, mirrors are aligned in a Kirkpatrick–Baez (KB) geometry, which allows the two-dimensional focusing of the source. The center of the horizontal mirror is placed 50 cm from the source, and the vertical mirror is 2 cm downstream of the horizontal mirror. The materials used in the design of each lane of the mirrors are summarized in Table 1. The coating material was chosen such that the reflectivity in the given energy range was optimized to a value $> 60\%$ for each mirror surface. The reflectivity curves were calculated using the software IMD [19] assuming a surface roughness of 1 nm.

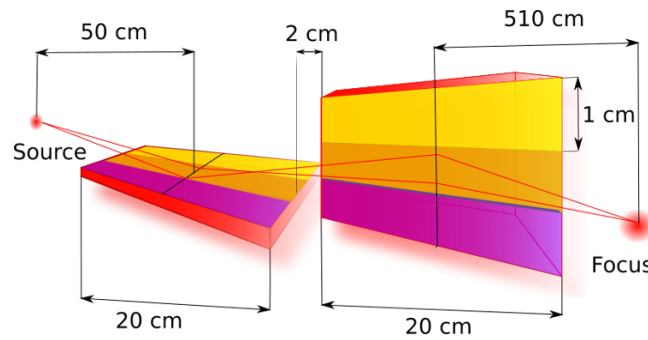


Figure 5. The geometrical configuration of the KB mirror system as used in the simulation.

X-ray reflectivities with other standard coating materials such as platinum, ruthenium, and rhodium were also simulated in order to test the performance of the mirror system. The choice of iridium over other materials for the first lane was due to its superior reflectivity at energies below 10 keV. The choice of material, the number of periods, and the thickness of the other lanes were to optimize the reflectivity and the width of the energy band covered by the lanes. The reflectivity presented here was calculated with silicon as the substrate material. A thorough scan of the reflectivity with other substrates such as SiO₂ was performed, and no significant difference in the reflectivity was found. The choice of silicon was made owing to its more favorable material properties such as thermal conductivity, thermal expansion coefficient, and lack of internal stress [20]. Moreover, with the state-of-the-art polishing techniques, silicon substrates can be polished to a surface roughness of less than 3 Å, which overall makes the optical performance of the mirror better.

Table 1. A summary of the coatings used for different lanes of the mirror and the corresponding reflectivity calculated at a grazing incidence angle of 5 mrad.

Lane	Transmission Efficiency (srad)	Layer Thickness Ir/Cr (nm)	Number of Periods	Energy Band (in keV) with Reflectivity > 0.6
1	9.6×10^{-3}	40/10	1	1–15
2	6.1×10^{-3}	5/5	5	15–18
3	6.8×10^{-3}	3.7/3.7	10	18–23

2.3. Geometrical Simulation

With the proper coating material identified and the corresponding reflectivity curves calculated, we performed a ray-tracing simulation in order to estimate the efficiency of the mirror system. All the geometrical ray-tracing simulation results reported here were calculated using the software OASYS [21]. The geometrical configuration for the simulation is shown in Figure 5. The geometrical parameters of each mirror of the KB mirror system used in the simulation are summarized in Table 2. The image plane of the mirror was set to be ~510 cm, which effectively magnifies the source ~10 times to a focal spot of roughly 100 μm. The magnification of the source enables probing enough of the sample volume to generate interpretable diffraction and spectroscopy data and in addition makes the beam more collimated, which is crucial in some experiments such as wide-angle X-ray diffraction and scattering.

We can estimate an effective acceptance angle of the *i*-th lane of the mirror analytically as $\Omega_i = \theta_i \cdot L/d_j$, where θ_i is the grazing incidence angle, *L* the length of the mirror, and *d_j* the mean distance of the mirrors from the source. The transmission efficiency of the mirror was obtained by multiplying the effective acceptance angle by the reflection efficiency of the mirror (η_{kb}). The reflection efficiency at the given photon energy was obtained by multiplying the reflectance of the two mirrors considering double reflection. Hence, the transmission efficiency is given by $T_i = \Omega_i \cdot (\eta_{kb})_i$. The transmission efficiency for each lane

for of the mirror system is summarized in Table 1, and corresponding reflectivity efficiency is shown in Figure 6.

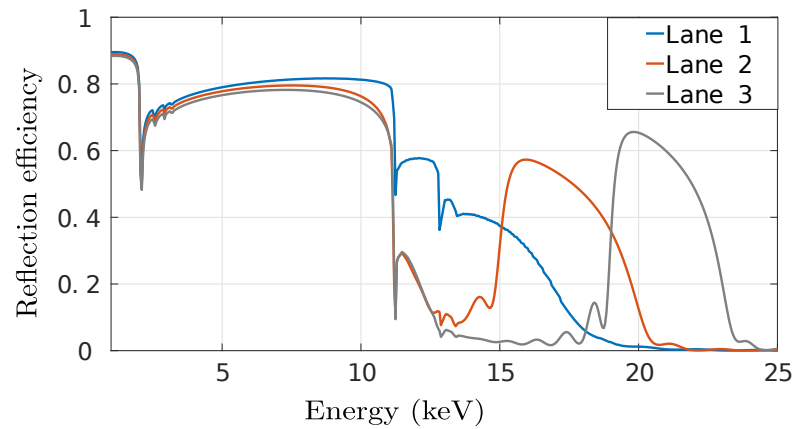


Figure 6. The reflection efficiency of the KB mirror system for three different lanes calculated at a grazing incidence angle of 5 mrad.

Table 2. Summary of the geometrical parameters of the mirrors.

Parameters	First Mirror	Second Mirror
Semi-major axes (cm)	291	291
Semi-minor axes (cm)	0.815	0.958
Source mirror distance (cm)	50	72
Mirror to focus distance (cm)	532	510
Grazing incidence (mrad)	5	5

The source was simulated in OASYS by using the beam profile generated from the 3D PIC simulation (Figure 4), specifying further spatial information such as source with a Gaussian intensity distribution with a $1/e^2$ radius of $3 \mu\text{m}$ (Figure 7 left) and an angular divergence of 14 mrad. The output intensity distribution at the focus of the KB mirror system is shown in Figure 7 right. Alternatively, the source can also be simulated by using the Wiggler parameters available within the OASYS software. Our experience has shown that these spectra are good enough to make a preliminary evaluation of the performance of the mirror with the betatron X-ray source. For a precise calculation, the PIC-generated input spectrum is preferred.

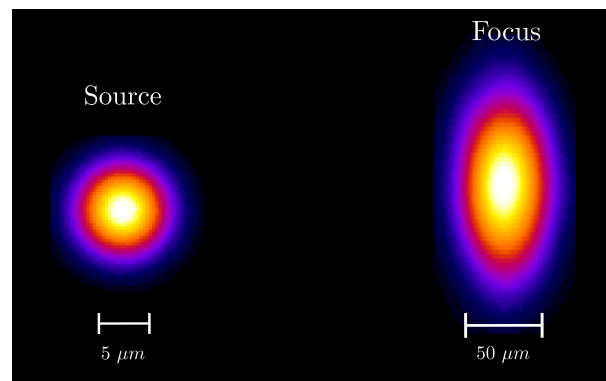


Figure 7. X-ray intensity distribution at the source (left) and at the focus (right) of the KB mirror system.

Using a PW-class laser as a driver with a 10 Hz repetition rate and with optimized laser and plasma conditions, the optimized betatron source can be expected to provide

photon flux up to 10^{14} photons/s. Using such a spectrum as an input in our KB mirror system, the number of photons at the sample plane for all three lanes can be well over 10^7 photons/s/0.1% of the bandwidth without any change in parameters of the X-ray source. The spectral flux distribution at the focus of each mirror lane after transmission through the KB system is reported in Figure 8. The flux at the focus can be enhanced by further reducing the divergence of the X-ray source below 5 mrad by using a passive plasma lens [8], which potentially upscales the photon number reaching the mirror system by a factor of 3. Such optimization is planned at the Gammatron beamline.

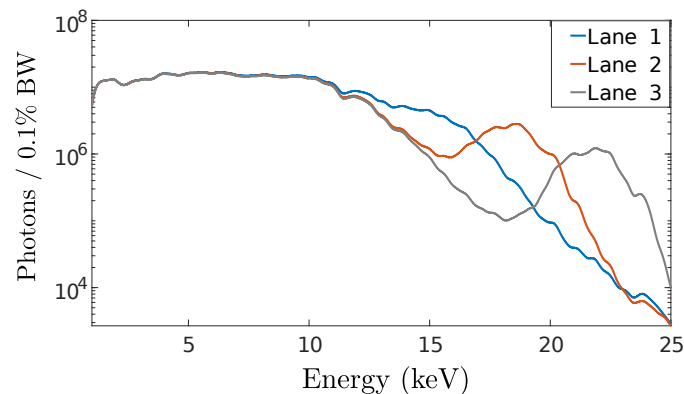


Figure 8. Spectral flux (per shot) at the focus after transmission through the KB system.

The thermal load should not affect the performance of the mirrors. Within the 10 Hz operation, the pulse energy of 5.6 mJ, and 2% of photons reaching the first mirror, the power density on the mirror is $\sim 9.9 \times 10^{-3} \text{ Wcm}^{-2}$. The thermal expansion coefficient and thermal conductivity of silicon at room temperature are $2.6 \times 10^{-6} \text{ K}^{-1}$ and $1.3 \text{ Wcm}^{-1} \text{ K}^{-1}$, respectively. The thermal slope error can be calculated using the formula $\Delta\alpha = \frac{\alpha P b}{\kappa}$ [22], where α is the thermal expansion coefficient, κ is the thermal conductivity, P is the power density, and b is the mirror length. For the system presented here, the calculated thermal slope error was 396 nrad, and thus, we did not expect detrimental influence on the optical performance of the mirror [23].

Design of the Mirror Mounting System

A mirror mount for the type of the mirror discussed above was designed. The mount shall be placed on the optical bench such that the center of the first mirror is 50 cm downstream of the source. Immediately before the mirror mount, an infrared (IR) rejection system (replenishable polyimide tape drive that acts as a plasma mirror deflecting the rest of the undepleted laser energy) will be placed to prevent heating of the mirrors by the residual laser radiation. The electron beam is deflected using a high-field permanent dipole magnet (1 T, 20 cm). A complete description of the entire system is given elsewhere [13]. The design of the mirror mount system was performed in such a way that each mirror is mounted on a stage with 5 degrees of freedom, which provides precise motions in three linear axes and two rotational axes. All the stages shall be equipped with encoders for precise position readings. Both stages are mounted on additional three-axis stages, which provide the necessary coarse movement to the mirror. The schematic of the mirror mounting system is shown in Figure 9.

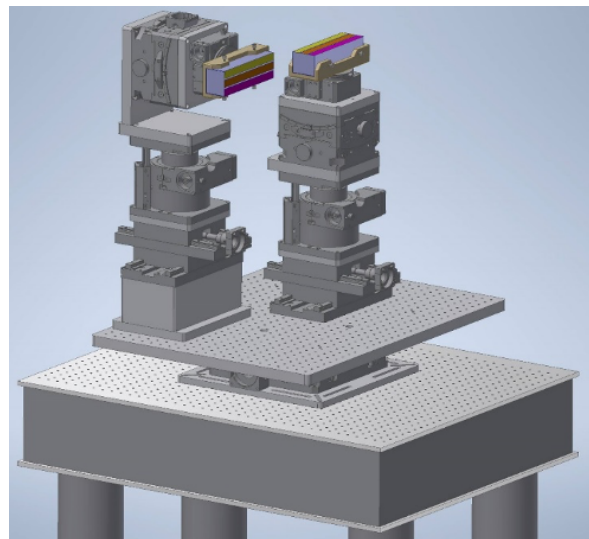


Figure 9. A schematic of the mirror mount for the KB mirror system.

3. Discussion

In all previously reported experiments with betatron X-rays, either a single reflecting surface such as a toroidal mirror [24] or grazing incidence mirror [25] for selected spectral wavelength was used. This offers limited flexibility during the experiment, especially when a wide spectral scan is necessary for the experiment. Additionally, when diverse applications are planned within the same beamline, changing the mirror system aligning them is a major part of the experimental time. An instance of tunable grazing incidence KB mirror has been demonstrated previously [26,27]. However, such mirror systems are far less efficient at higher energies. The introduction of multi-lane mirrors partially solves all these issues. The multi-lane mirror proposed here comprises lanes with a single-layer coating and multilayer coating optimized to obtain the flux at the given energy range. This assists in better exploiting the source for different applications ranging from the spectroscopy of light to heavy elements, the diffraction of bulk samples and biomolecular crystals, phase-contrast imaging, and other coherent and incoherent structural and imaging methods.

The geometrical simulation shows that the X-ray transport to the sample with a loss of less than three orders of magnitude for the energy ranging from 1–23 keV is achievable. While the reflective loss accounts for the loss of less than 65% of the incoming photons, the geometrical loss is significant. With the physical constraint of placing the mirror closer to the source and making large mirrors, the optimization of the source divergence will be crucial in reducing the geometrical loss. Nevertheless, the total efficiency of our design is significantly higher than any other optical system previously used for betatron X-rays.

In addition, by increasing the incidence angle, the Bragg peaks' thickness is reduced, essentially achieving monochromatization of the X-ray beam near the vicinity of the Bragg peak, which can especially be attractive for diffraction experiments. Even though reflectivity from these peaks is diminished for higher grazing angles, the extra photons captured by the mirror make up for the loss according to our calculations. For example, for a grazing angle of 20 mrad, we obtained an FWHM of Bragg's peak 0.8 keV and sixteen-times more photons incident on the mirror, but the reflectivity was reduced four times on each mirror, giving the same number of photons as for 5 mrad.

4. Conclusions

In conclusion, we designed a multi-lane KB mirror as an efficient optical system for focusing the betatron X-rays up to 23 keV. With a focal spot size of 100 μm , it would permit enough volume of the sample to be probed by X-rays. For the proposed multi-lane mirror, the coating layers' thickness and the number of layers were optimized. For each lane of

the mirror, the reflectivity was set to be higher than 60%. We also performed a geometrical simulation to estimate the number of photons at the sample plane. From our simulations, the total efficiency of the mirror system was determined to be better than $\sim 0.5\%$ for all lanes. A similar mirror system shall be installed at the hard X-ray station of the Gammatron X-ray beamline at the ELI Beamlines facility. Additionally, our work also demonstrates that the existing open-source software can be used to design and calibrate the proper optical element for laser-driven betatron radiation. We believe that the installation of such optics at the user-oriented betatron X-ray beamline shall accelerate the diverse applications to be explored with this ultrafast X-ray source.

Author Contributions: Conceptualization, U.C. and K.P.K.; X-ray optics simulation, M.R., U.C. and K.P.K.; PIC simulation, M.L.; writing—original draft preparation, K.P.K., M.R. and U.C.; writing—review and editing, M.L., U.C. and J.N.; supervision, U.C. and K.P.K. All authors have read and agreed to the published version of the manuscript.

Funding: We acknowledge the funding from the projects “Advanced re- search using high-intensity laser produced photons and particles” (CZ.02.1.01/0.0/0.0/16_019/0000789) and “Structural Dynamics of Biomolecular Systems” (ELIBIO) (CZ.02.1.01/0.0/0.0/15_003/0000447) from the European Regional Development Fund. The work was also supported by funding from the large infrastructures (LM2018141). K.K. acknowledges financial support from the Czech Academy of Sciences (grant number MSM100101901).

Data Availability Statement: Data available upon reasonable request to corresponding author.

Conflicts of Interest: The authors declare no conflict of interest.

References

- Gaffney, K.; Chapman, H.N. Imaging atomic structure and dynamics with ultrafast X-ray scattering. *Science* **2007**, *316*, 1444–1448. [[CrossRef](#)] [[PubMed](#)]
- Bargheer, M.; Zhavoronkov, N.; Woerner, M.; Elsaesser, T. Recent progress in ultrafast X-ray diffraction. *Chemphyschem Eur. J. Chem. Phys. Phys. Chem.* **2006**, *7*, 783–792. [[CrossRef](#)] [[PubMed](#)]
- Bressler, C.; Chergui, M. Molecular structural dynamics probed by ultrafast X-ray absorption spectroscopy. *Annu. Rev. Phys. Chem.* **2010**, *61*, 263–282. [[CrossRef](#)]
- Rousse, A.; Phuoc, K.T.; Shah, R.; Pukhov, A.; Lefebvre, E.; Malka, V.; Kiselev, S.; Burgy, F.; Rousseau, J.P.; Umstadter, D.; et al. Production of a keV X-ray beam from synchrotron radiation in relativistic laser-plasma interaction. *Phys. Rev. Lett.* **2004**, *93*, 135005. [[CrossRef](#)]
- Kneip, S.; McGuffey, C.; Martins, J.L.; Martins, S.; Bellei, C.; Chvykov, V.; Dollar, F.; Fonseca, R.; Huntington, C.; Kalintchenko, G.; et al. Bright spatially coherent synchrotron X-rays from a table-top source. *Nat. Phys.* **2010**, *6*, 980–983. [[CrossRef](#)]
- Fourmaux, S.; Corde, S.; Phuoc, K.T.; Leguay, P.; Payeur, S.; Lassonde, P.; Gnedyuk, S.; Lebrun, G.; Fourment, C.; Malka, V.; et al. Demonstration of the synchrotron-type spectrum of laser-produced Betatron radiation. *New J. Phys.* **2011**, *13*, 033017. [[CrossRef](#)]
- Tajima, T.; Dawson, J.M. Laser electron accelerator. *Phys. Rev. Lett.* **1979**, *43*, 267. [[CrossRef](#)]
- Svensson, J.B.; Guénot, D.; Ferri, J.; Ekerfelt, H.; González, I.G.; Persson, A.; Svendsen, K.; Veisz, L.; Lundh, O. Low-divergence femtosecond X-ray pulses from a passive plasma lens. *Nat. Phys.* **2021**, *17*, 639–645. [[CrossRef](#)]
- Fourmaux, S.; Hallin, E.; Chaulagain, U.; Weber, S.; Kieffer, J. Laser-based synchrotron X-ray radiation experimental scaling. *Opt. Express* **2020**, *28*, 3147–3158. [[CrossRef](#)] [[PubMed](#)]
- Kozlova, M.; Andriyash, I.; Gautier, J.; Sebban, S.; Smartsev, S.; Jourdain, N.; Chulagain, U.; Azamoum, Y.; Tafzi, A.; Goddet, J.P.; et al. Hard x rays from laser-wakefield accelerators in density tailored plasmas. *Phys. Rev. X* **2020**, *10*, 011061. [[CrossRef](#)]
- Lamač, M.; Chaulagain, U.; Jurkovič, M.; Nejdil, J.; Bulanov, S. Two-color nonlinear resonances in betatron oscillations of laser accelerated relativistic electrons. *Phys. Rev. Res.* **2021**, *3*, 033088. [[CrossRef](#)]
- Rus, B.; Bakule, P.; Kramer, D.; Naylor, J.; Thoma, J.; Green, J.; Antipenkov, R.; Fibrich, M.; Novák, J.; Batysta, F.; et al. ELI-Beamlines: Development of next generation short-pulse laser systems. In *Research Using Extreme Light: Entering New Frontiers with Petawatt-Class Lasers II*; International Society for Optics and Photonics: Bellingham, WA, USA, 2015; Volume 9515, p. 95150F.
- Chaulagain, U. ELI Gammatron Beamline: Dawn of ultrafast hard X-ray science. *to be published*.
- Gruse, J.N.; Streeter, M.; Thornton, C.; Armstrong, C.; Baird, C.; Bourgeois, N.; Cipiccia, S.; Finlay, O.; Gregory, C.; Katzir, Y.; et al. Application of compact laser-driven accelerator X-ray sources for industrial imaging. *Nucl. Instrum. Methods Phys. Res. Sect. A Accel. Spectrometers Detect. Assoc. Equip.* **2020**, *983*, 164369. [[CrossRef](#)]
- Chaulagain, U.; Bohacek, K.; Kozlova, M.; Nejdil, J.; Krus, M.; Horny, V.; Mahieu, B.; Ta-Phuoc, K. X-ray phase contrast imaging of biological samples using a betatron X-ray source generated in a laser wakefield accelerator. In *Laser Acceleration of Electrons, Protons, and Ions IV*; International Society for Optics and Photonics: Bellingham, WA, USA, 2017; Volume 10240, p. 1024014.

16. Kettle, B.; Gerstmayr, E.; Streeter, M.; Albert, F.; Baggott, R.; Bourgeois, N.; Cole, J.; Dann, S.; Falk, K.; González, I.G.; et al. Single-shot multi-keV x-ray absorption spectroscopy using an ultrashort laser-wakefield accelerator source. *Phys. Rev. Lett.* **2019**, *123*, 254801. [[CrossRef](#)]
17. Arber, T.; Bennett, K.; Brady, C.; Lawrence-Douglas, A.; Ramsay, M.; Sircombe, N.; Gillies, P.; Evans, R.; Schmitz, H.; Bell, A.; et al. Contemporary particle-in-cell approach to laser-plasma modelling. *Plasma Phys. Control. Fusion* **2015**, *57*, 113001. [[CrossRef](#)]
18. Jackson, J.D. *Classical Electrodynamics*, 3rd ed.; John Wiley & Sons: New York, USA, 1999.
19. Windt, D.L. IMD—Software for modeling the optical properties of multilayer films. *Comput. Phys.* **1998**, *12*, 360–370. [[CrossRef](#)]
20. Riveros, R.E.; Biskach, M.P.; Allgood, K.D.; Kearney, J.D.; Hlinka, M.; Numata, A.; Zhang, W.W. Fabrication of monocrystalline silicon X-ray mirrors. In *Optics for EUV, X-ray, and Gamma-ray Astronomy IX*; O'Dell, S.L., Pareschi, G., Eds.; International Society for Optics and Photonics, SPIE: Bellingham, WA, USA, 2019; Volume 11119, pp. 47–54. [[CrossRef](#)]
21. Rio, M.S.D.; Rebuffi, L. OASYS: A software for beamline simulations and synchrotron virtual experiments. *AIP Conf. Proc.* **2019**, *2054*, 060081.
22. Freund, A.K.; de Bergevin, F.; Marot, G.; Riekkel, C.; Susini, J.; Zhang, L.; Ziegler, E. X-ray mirrors for the European Synchrotron Radiation Facility. *Opt. Eng.* **1990**, *29*, 928–941.
23. Bennett, H.E.; Khounsary, A.M. Comparison of technology for high-power laser mirrors and synchrotron radiation mirrors. In *High Heat Flux Engineering II*; Khounsary, A.M., Ed.; International Society for Optics and Photonics, SPIE: Bellingham, WA, USA, 1993; Volume 1997, pp. 257–275. [[CrossRef](#)]
24. Ta Phuoc, K.; Fitour, R.; Tafzi, A.; Garl, T.; Artemiev, N.; Shah, R.; Albert, F.; Boschetto, D.; Rousse, A.; Kim, D.; et al. Demonstration of the ultrafast nature of laser produced betatron radiation. *Phys. Plasmas* **2007**, *14*, 080701. [[CrossRef](#)]
25. Mo, M.; Fourmaux, S.; Ali, A.; Lassonde, P.; Kieffer, J.C.; Fedosejevs, R. Characterization of laser wakefield generated betatron X-ray radiation using grazing incidence mirror reflection. *Eur. Phys. J. D* **2014**, *68*, 301. [[CrossRef](#)]
26. Mo, M.; Chen, Z.; Fourmaux, S.; Saraf, A.; Otani, K.; Kieffer, J.; Tsui, Y.; Ng, A.; Fedosejevs, R. Laser wakefield generated x-ray probe for femtosecond time-resolved measurements of ionization states of warm dense aluminum. *Rev. Sci. Instrum.* **2013**, *84*, 123106. [[CrossRef](#)]
27. Zeraouli, G.; Gatti, G.; Longman, A.; Pérez-Hernández, J.; Arana, D.; Batani, D.; Jakubowska, K.; Volpe, L.; Roso, L.; Fedosejevs, R. Development of an adjustable Kirkpatrick-Baez microscope for laser driven X-ray sources. *Rev. Sci. Instrum.* **2019**, *90*, 063704. [[CrossRef](#)]